Eur. Phys. J. B **39**, 5–17 (2004)
DOI: 10.1140/epjb/e2004-00164-3

THE EUROPEAN PHYSICAL JOURNAL B

Structural, electronic, and optical properties of beryllium monochalcogenides

C.M.I. Okoye[a]

Department of Physics and Astronomy, University of Nigeria, Nsukka, Nigeria

Received 26 September 2003
Published online 18 June 2004 –

Abstract. The results of first-principles theoretical study of the structural, electronic and optical properties of beryllium monochalcogenides BeTe, BeSe and BeS, performed using the full potential linearized augmented plane wave (FP-LAPW) method are presented. The calculated structural parameters and band gaps compare very well with previous theoretical results. The trends of the band gap pressure coefficients and volume deformation potentials for these II-VI compounds are investigated. The linear pressure coefficients for the $\Gamma-$X and $\Gamma-\Gamma$ band gaps increase with decrease in anion atomic weight. The dependence of the direct and indirect band gaps on the relative change of lattice constant are found to follow almost the same type of trends in each of these compounds. The volume deformation potential (a_v^α) for the direct ($\alpha = \Gamma-\Gamma$) and indirect ($\alpha = \Gamma - L$) gaps are positive, but negative for the indirect ($\Gamma-$X) gap. Furthermore, a_v^α, for $\alpha = \Gamma-$X transitions decreases with increase in anion atomic number whereas $a_v^{\Gamma-\Gamma}$, increases. The optical properties have also been calculated. From the reflectivity spectra, the compounds will be useful for optical applications. The variation of the band gaps with respect to the application of pressure and the origin of some of the peaks in the optical spectra are discussed in terms the calculated electronic structure.

PACS. 71.15.Ap Basis sets (LCAO, plane-wave, APW, etc.) and related methodology (scattering methods, ASA, linearized methods, etc.) – 71.15.Mb Density functional theory, local density approximation, gradient and other corrections – 71.20.Nr Semiconductor compounds

1 Introduction

The beryllium monochalcogenides BeTe, BeSe and BeS are II-VI compounds which crystallize at low pressure in the four-fold coordinated zinc-blende structure. Apart from BeO and MgTe, which crystallize in the hexagonal wurzite structure, all the other group-IIa chalcogenides adopt the cubic rocksalt structure. A distinguishing feature in the beryllium compounds is that the cations (Be ions) are extremely small as compared to the anions except BeO [1]. This leads to an excess of the critical ratio of ionic radii, 4.45, for the zincblende structures in all three Be compounds; BeS, BeSe and BeTe. Thus, unlike other IIa-VI compounds which are ionic, Be chalcogenides exhibit a high degree of covalent bonding with the Philips ionicities ranging from 0.169 in BeTe to 0.312 in BeS [2]. The beryllium monochalcogenides are semiconductors with indirect fundamental band gap associated with $\Gamma-$X transitions. Also, BeS has high hardness while BeTe is a small gap semiconductor. These interesting properties make them potentially useful for technological applications. Therefore, there is renewed interest in these compounds which could be used in building green and blue light emitting electro-optical devices [3].

To date, probably as a result of their very high toxic nature which makes it difficult to obtain them as single crystals or epitaxial layers, only few experimental studies [4–6] have been performed on these compounds and consequently, only a few theoretical studies of these compounds are available in the literature [9–15]. In addition, the band gap pressure coefficients of these compounds are not well-known. The only available theoretical studies [12,13] were performed using first-principles pseudopotential calculations.

The first theoretical study on these compounds were performed by Stukel [9]. He used Slater's local-exchange potential approach to perform a non-relativistic self-consistent calculation of the band structure and dielectric function of BeTe, BeSe and BeS. This was followed by Sakar and Chatterjee [10] who used the composite wave variational version of the augmented plane wave (APW) method in conjunction with the linear combination of atomic orbitals (LCAO) interpolation scheme to compute the energy band structure and joint density of states of the compounds at various symmetry points and axes of the Brillouin zone. Subsequently, Munoz et al. [11] calculated the band structure and relative stability of high temperature phases using a first principles pseudopotential method based on density functional formalism and local density approximation (LDA). Van Camp and Van Doren

[a] e-mail: okoyecmi@yahoo.com

[12] also used density functional theory together with pseudopotential technique to study the ground-state properties and structural phase transitions of beryllium sulphide. The work of Gonzalez-Diaz et al. [13] employed the first-principles pseudopotential method based on the density functional theory and used the Cerperly Alder form of the local density approximation for the exchange-correlation as parametrized by Perdew and Zunger. Fleszar and Hanke [14] employed the ab initio GW-approach to study the band structure of the compounds. The energy gaps they obtained are in better agreement with available experimental data than the results of some previous theoretical results [11–13]. In a more recent study, Benosman et al. [15], used the LAPW method employing the local density approximation for exchange and correlation to study the structural and electronic properties of BeS. The discrepancy could be attributed to the LDA problem of underestimation of the energy gap.

It has been demonstrated recently that due to the high degree of covalent bonding and bond energy which should entail a lattice hardening and slower degradation with time, interest in the beryllium compounds have been renewed. However, among their optical properties, only the dielectric function have been properly studied. The technique of spectroscopic ellipsometry (SE) facilitates the direct determination of the complex dielectric function $\varepsilon = \varepsilon_1 + i\varepsilon_2$ and gives both the real and imaginary parts of the dielectric function without having to employ a Kramers-Kronig transformation. Such measurements have recently been performed by Wilmers et al. [7,8] in the ultra violet (UV) and vacuum ultra violet (VUV) range. To this end, we shall use the SE measurements to evaluate how well our theoretical approach successfully accounts for the dielectric function and other optical properties. At the moment there are no first-principles studies of most of the optical properties. of zincblende beryllium chalcogenides. As such, our study will help provide a theoretical data base for these compounds. In the present study, the electronic structure and optical properties of beryllium chalcogenides BeTe, BeSe and BeS in the zincblende structure are calculated using full-potential linearized augmented plane wave (FP-LAPW) method within the density functional formalism using the generalized gradient approximation (GGA). It is known [16] that the GGA has stronger theoretical foundation because it accounts specifically for density gradients that are neglected in local density approximation (LDA), and does so in a way that satisfies several exact constraints in the form of the exchange-correlation energy functional. It is therefore appropriate to use GGA in this study employing a full-potential electronic structure method. The paper is organized as follows: Section 2, briefly describes the computational details regarding the methods used in our calculation of the electronic and optical properties. In Section 3, the FP-LAPW results for the structural properties, band structure, band gap pressure coefficient, and optical properties are presented and compared with available experimental data and other theoretical calculations. Finally, conclusions are given in Section 4.

2 Method of calculation

We will study the structural, electronic and optical properties of zincblende BeTe, BeSe and BeS using the WIEN97 package [17]. This program employs a scalar relativistic full-potential linearized augmented plane wave (FP-LAPW) method with correlations and exchange effects treated using the generalized gradient approximation (GGA) of Purdue, Burke and Ernzenhof [18] within the density functional theory [19]. The package employs a basis set achieved by dividing the unit cell into non-overlapping atomic spheres (centered at the atomic sites) and an interstitial region. In the atomic sphere, a linear combination of radial functions times spherical harmonics is used and in the interstitial region, a plane wave expansion is augmented by an atomic-like function in every atomic sphere. This approach has been extensively tested and is among the most accurate methods for performing electronic structure calculations for crystals. In our calculations, the sphere radii of Be, Te, Se and S have been chosen as 1.5, 2.3 2.0 and 1.9 atomic units respectively. Within these spheres, the charge density and potential are expanded in terms of crystal harmonics. The Brillouin zone integrations have been carried out with a total of $30k$-points in the irreducible Brillouin zone. The calculations are iterated to self-consistency with specified charge convergence criterion and parameter $R_{MT}K_{max}$ (where R_{MT} is the atomic sphere radii and K_{max} is the interstitial plane wave cut-off) was set to 8.0.

The pressure dependence of the energy gap for the beryllium chalcogenides were calculated using the following equation [20]:

$$\left(\frac{\partial E_g}{\partial P}\right)_T = \left(\frac{\partial E_g}{\partial V}\right)_T \left(\frac{\partial V}{\partial P}\right)_T = -\frac{V_0}{B_0}\left(\frac{\partial E_g}{\partial V}\right)_T. \quad (1)$$

The value of $(\partial E_g/\partial V)_T$ was obtained directly from the energy gap versus volume calculations, and the value of $(\partial V/\partial P)_T$ was obtained from the compressibility relationship:

$$K = \frac{1}{B_0} = -\frac{1}{V_0}\left(\frac{\partial V}{\partial P}\right)_T \quad (2)$$

where V_0 is the equilibrium volume and B_0 is the theoretical bulk modulus at the equilibrium volume. The theoretical bulk modulus used in this study is calculated as described in Section 3.1.

For the calculation of the optical properties, a dense mesh of uniformly distributed k-points is required. Hence, the Brillouin zone integration was performed using the tetrahedron method with many more k-points in the irreducible part of the Brillouin zone without broadening. The dielectric function

$$\varepsilon(\omega) = \varepsilon_1(\omega) + i\varepsilon_2(\omega) \quad (3)$$

is known to describe the optical response of the medium at all photon energies $E = \hbar\omega$. In this study, the imaginary part of the dielectric function is given as in

Table 1. Calculated lattice constant (a_0), bulk modulus (B_0), and first pressure derivative of bulk modulus ($B_0^{'}$) for beryllium chacogenides, BeTe, BeSe and BeS. Results are compared with available experimental data and previous calculations.

BeTe	Lattice constant (Å)	B_0 (GPa)	$B_0^{'}$
Present study	5.663(a_0)	57.66	6.21
Experiment(Used in this study)	5.627[1]		
	5.617[2]	67.0[2]	
Other calculations	5.531[3]	70.0[3]	
	5.625[2]	66.8[2]	
	5.631[2]	68.2[2]	3.4[2]
BeSe			
Present study	5.178(a_0)	74.97	4.02
Experiment (used in this study)	5.144[1]		
	5.139[2]	92.2[4]	
Other calculations	5.037[2]	92.2[2]	3.7[2]
	5.037[3]	98.0[3]	
BeS			
Present study	4.887(a_0)	92.23	3.70
Experiment (used in this study)	4.863[1]		
	4.865[2]		
Other calculations	4.745[2]	116.0[3]	
	4.745[2]	113.4[2]	3.5[2]
	4.773[5]	101.9[5]	3.71[5]

[1] See reference [14], [2] see reference [11], [3] see reference [13], [4] see reference [1], [5] see reference [12].

reference [21] by

$$\varepsilon_2(\omega) = \left(\frac{4\pi^2 e^2}{m^2\omega^2}\right) \sum_{i,j} \int \langle i|M|j\rangle^2 f_i\,(1-f_j) \times \delta\,(E_f - E_i - \omega)\; d^3k \quad (4)$$

where M is the dipole matrix, i and j are the initial and final states respectively, f_i is the the Fermi distribution function for the ith state, and E_i is the energy of electron in the ith state. The real part ($\varepsilon_1(\omega)$) of the dielectric function can be extracted from the imaginary part using the Kramers-Kronig relation in the form [21,22]

$$\varepsilon_1(\omega) = 1 + \frac{2}{\pi} P \int_0^\infty \frac{\omega^{'}\varepsilon_2(\omega^{'})d\omega^{'}}{(\omega^{'2} - \omega^2)} \quad (5)$$

where P implies the principal value of the integral.

The optical reflectivity spectra are derived from the Fresnel's formula for normal incidence assuming an orientation of the crystal surface parallel to the optical axis using the relation [21,23]

$$R(\omega) = \left|\frac{\sqrt{\varepsilon(\omega)} - 1}{\sqrt{\varepsilon(\omega)} + 1}\right|^2. \quad (6)$$

while the electronic energy-loss function (–Im($\frac{1}{\varepsilon}$)) is given by [22,24,25]

$$-\mathrm{Im}\left(\frac{1}{\varepsilon}\right) = \frac{\varepsilon_2(\omega)}{\varepsilon_1^2(\omega) + \varepsilon_2^2(\omega)}. \quad (7)$$

We calculate the absorption coefficient $I(\omega)$ and the real part of optical conductivity Re[$\sigma(\omega)$] using the following expressions [21,23]:

$$I(\omega) = 2\omega \left\{\frac{\sqrt{\varepsilon_1^2(\omega) + \varepsilon_2^2(\omega)} - \varepsilon_1(\omega)}{2}\right\}^{1/2} \quad (8)$$

$$\mathrm{Re}[\sigma(\omega)] = \frac{\omega\varepsilon_2}{4\pi}. \quad (9)$$

Also, the optical spectra such as the refractive index, $n(\omega)$, and the extinction coefficient, $k(\omega)$, are calculated in terms of the components of the complex dielectric function as follows [23–25]:

$$n(\omega) = \left\{\frac{\varepsilon_1(\omega)}{2} + \frac{\sqrt{\varepsilon_1^2(\omega) + \varepsilon_2^2(\omega)^2}}{2}\right\}^{1/2} \quad (10)$$

$$k(\omega) = \left\{\frac{\sqrt{\varepsilon_1^2(\omega) + \varepsilon_2^2(\omega)}}{2} - \frac{\varepsilon_1(\omega)}{2}\right\}^{1/2}. \quad (11)$$

3 Results and discussion

3.1 Structural parameters

The equilibrium lattice constant (a_0) has been determined by calculating the total energy at a number of lattice parameters around the experimental value within the FP-LAPW method in scalar relativistic calculations (without spin-orbit coupling effects). To achieve this, we have chose the most recent values of the lattice constants [14]. Fitting of the Murnaghan equation of state [26] to the total energies versus lattice parameters, yields the equilibrium lattice parameter (a_0), bulk modulus, B_0, and the pressure derivative of the bulk modulus, $B_0^{'}$. These are tabulated

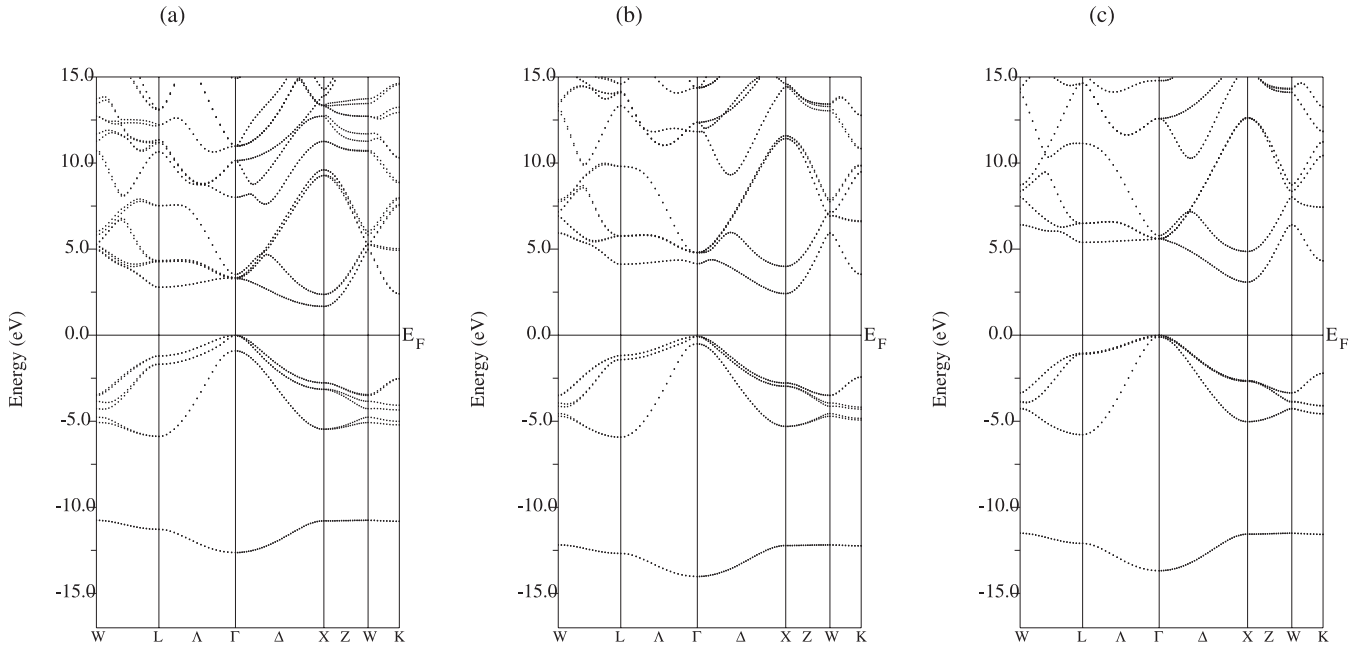

Fig. 1. Calculated relativistic electronic band structures of (a) BeTe (b) BeSe and (c) BeS. The valence band maximum is at zero.

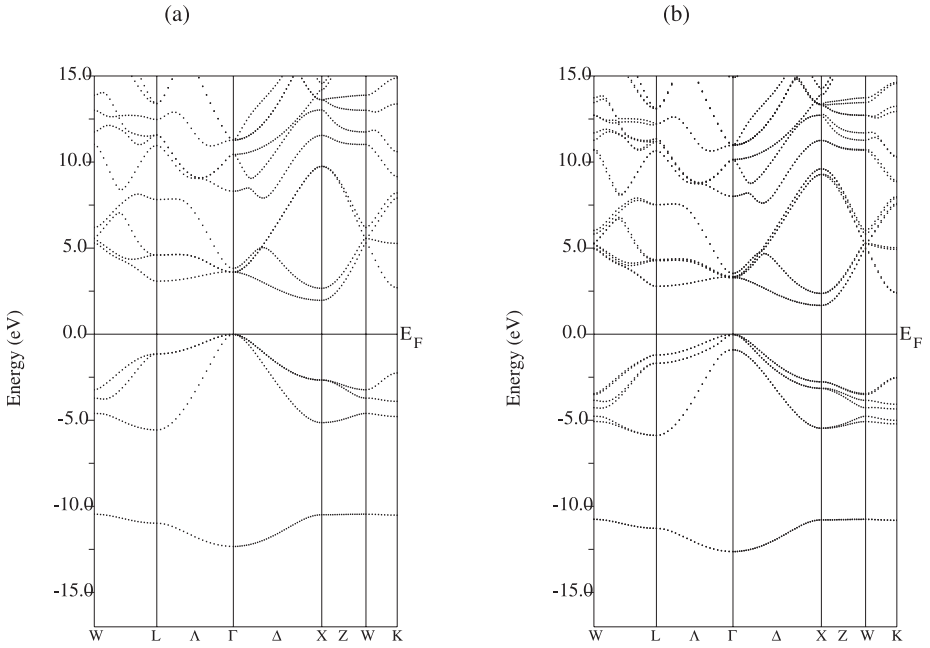

Fig. 2. Calculated electronic band structures of BeTe. (a) Semirelativistic and (b) relativistic. The valence band maximum is at zero.

in Table 1. It is seen that the structural parameters are in good agreement with results of previous studies and experiment. The small overestimation in the equilibrium lattice constant is a common feature with GGA calculations.

3.2 Band structure and density of states

Electronic band structure of zincblende beryllium chalcogenides BeTe, BeSe and BeS based on self consistent scalar relativistic FP-LAPW calculations in which the exchange and correlation were treated in the GGA along the symmetry lines of the face centered cubic Brillouin zone are plotted in Figure 1. It shows the relativistic (including spin-orbit coupling coupling) band structures of BeTe, BeSe and BeS while Figure 2 compares the band structures of BeTe calculated (a) scalar-relativistically and (b) fully relativistically. The calculations were performed at the experimental value of the lattice constant. A comparison of Figures 2a and 2b shows that the inclusion of spin

Table 2. Calculated energy gaps at high symmetry points in BeTe, BeSe and BeS.

		Energy-gap(eV)				
		Direct			Indirect	
	a (Å)	$\Gamma \rightarrow \Gamma$	X $\rightarrow$ X	L $\rightarrow$ L	$\Gamma \rightarrow$ X	$\Gamma \rightarrow$ L
BeTe						
Expt.	5.627	4.53[1]			2.8[2], 2.7[3]	
This work	5.627	3.62	4.63	4.23	1.98	3.129
Previous study						
	5.627				1.62[1]	
					2.89[4]	
					2.6[1]	
		3.68[5]			1.81[5]	
		3.68[6]			1.80[6]	
BeSe						
Expt.	5.144	5.55[7]				
This work	5.144	4.37	5.29	5.41	2.63	4.339
Previous study						
		5.47[8]			3.61[4]	
		4.72[6]			2.39[6]	
BeS						
Expt.	4.863					
This work	4.863	5.65	5.74	6.46	3.13	5.437
Previous study						
		5.51[6]			2.75[6]	
					4.17[4]	
		5.397[9]			2.816[9]	
		5.503[10]			2.847[10]	

[1] M. Nagelstraber, H. Droge, H.P. Steinruck, F. Fischer, T. Litz, A. Waag, G. Landwehr, A. Flesser, W. Hanke, Phys. Rev. B **58**, 10394 (1998) and references therein; [2]see reference [9]; [3]R.G. Dandrea, C.B. Duke, Appl. Phys. Lett. **64**, 2145 (1994); [4]see reference [9]; [5]see reference [11]; [6]see reference [13]; [7]see reference [8]; [8]see reference [14]; [9]see reference [12]; [10]see reference [15].

orbit coupling lifts the degeneracy in the valence band. This is strongest in BeTe. The overall band profiles are found to be in fairly good agreement with previous theoretical results. In all the cases, the valence band maximum occurs at the Γ-point while the conduction band minimum occurs at the X-point and these are accurately located by our calculations. Thus the energy gap is indirect between the top of the (anion p) valence band and the bottom of the conduction band at the X-point. Note that the chalcogen p bands shift up in energy going from the sulphide to the telluride. This is the normal behaviour related to the increase of the lattice parameters, which was also found for other II-VI compounds [27,28] The band gaps displayed in Table 2 were deduced from the fully relativistic calculations. It is seen that the theoretically calculated results are in fair agreement with previous studies [11,13]. However, the band gaps are on the whole underestimated in comparison with the experimental results. This is typical error arising due to the Kohn-Sham formalism and the GGA approximation. The band gap problem is considered to arise due to lack of non-locality and energy dependence in the exchange-correlation scheme used in the density functional formalism [29].

We note that the order of the band gaps E_g(BeS) > E_g(BeSe) > E_g(BeTe) is anomalous. The trend in II-VI semiconductors is that the band gaps decrease monotonically with the anion atomic number [27]. Furthermore, the calculated valence band widths are 12.3 eV, 13.8 eV and 13.63 eV for BeTe, BeSe and BeS respectively in good agreement with previous studies [13,15]. The result shows that the valence band width is maximum for BeSe. Showing that the wave function is more localized for BeS than for BeTe. This is in line with the usual trend in which the valence band states become more localized as a material becomes less covalent and more ionic, as it does when we decrease the atomic number of the anion. It is also noticed that the band gap between the lowest band (anion s band) and the valence band is least in BeTe due to the higher energy position of tellurium s band.

In Figure 3, we have displayed the total density of states of the beryllium compounds BeTe, BeSe and BeS calculated at the experimental lattice constant. We have used the site and angular momentum decomposed density of states (not shown) to identify the character of the band states for these compounds. It is seen that for each compound, the bands above the zero of energy are

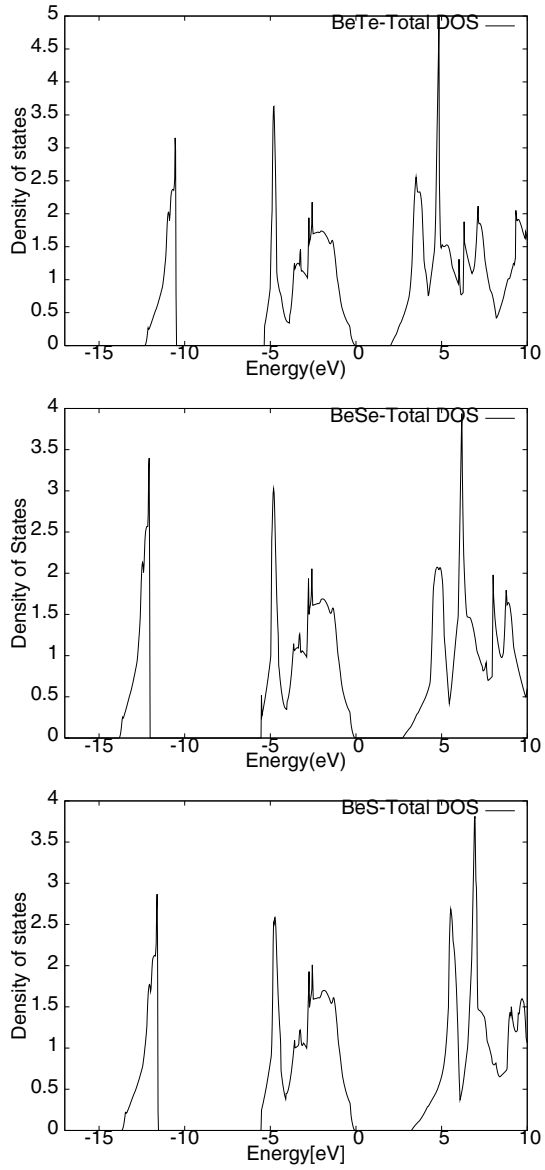

Fig. 3. Total DOS for zincblende beryllium chalcogenides BeTe, BeSe and BeS.

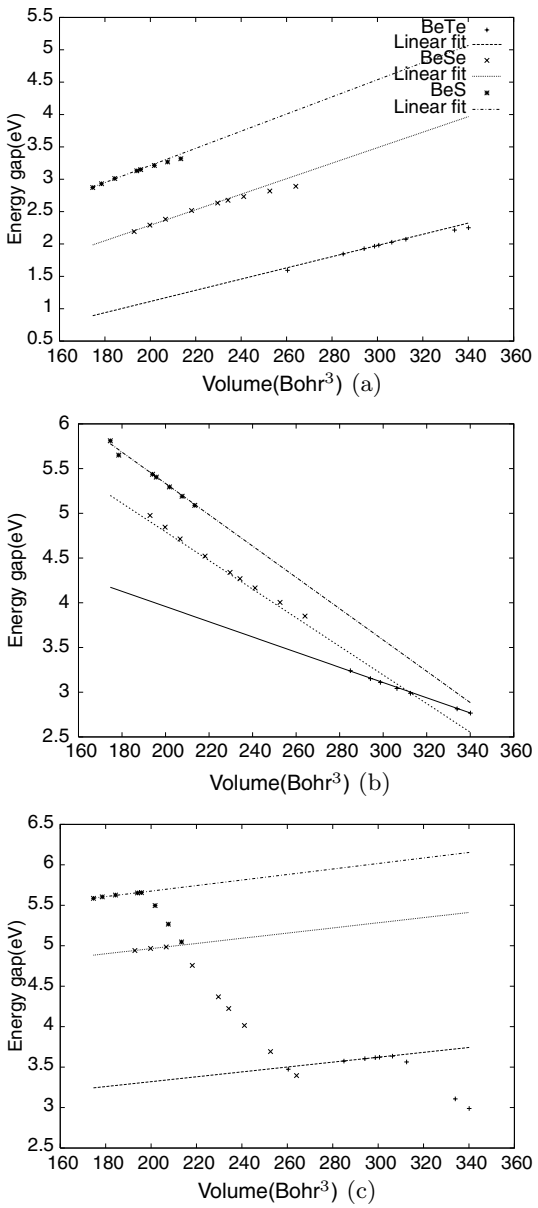

Fig. 4. Theoretical dependence of the (a) indirect ($\Gamma_v - X_c$) band gap, (b) ($\Gamma_v - L_c$) and (c) direct ($\Gamma_v - \Gamma_c$) of for beryllium chalcogenides (a) BeTe (b) BeSe and (c) BeS as a function of atomic volume. The legend for (a) also applies to (b) and (c).

predominantly of anion and cation p-character but also with some anion s and cation-d content. Just below the zero of energy, the bands have chalcogen p-character. The lower valence states are formed by mixture of Be-s and chalcogen-p states. The lowest band in the figures is nearly exclusively of chalcogen atom s character.

4 Pressure dependence of energy bands

We are aware that the GGA within the density functional formalism, underestimates the band gaps compared with experiment [30,31]. However, despite this shortcoming of the GGA, the pressure derivatives or the deformation potentials of band gaps in semiconductors are accurately calculated in the GGA(or LDA) and do not depend on the type or functional form of the exchange-correlation potential [30,32,33]. As such, we have investigated the pressure dependence of the energy gap for beryllium chalcogenides using the FP-LAPW method within the generalized gradient approximation. In order to achieve this, we first determine the volume dependence of the energy gaps of the compounds. These are shown in Figure 4. The volume dependence is obtained from the slope of the linear region which lies below the equilibrium volume. We have fitted the region below the equilibrium volume with linear function following the procedure in reference [20]. The straight lines are drawn using the values of the linear fit. The slope $\frac{dE_g}{dV}$ of the lines are given in Table 3. Using these values as well as the equilibrium volume V_0 and theoretical bulk

Table 3. Calculated values of the pressure coefficients ($\frac{dE_g}{dV}$) and and volume deformation potentials ($\frac{dE_g}{d\ln V}$) for beryllium chacogenides, BeTe, BeSe and BeS. Results are compared with available experimental data and previous calculations.

	$\frac{dE_g}{dV}$(meV(Bohr)$^{-3}$)	$\frac{dE_g}{dP}$(meV(GPa)$^{-1}$)	$\frac{dE_g}{d\ln V}$(eV)
BeTe			
$\Gamma \rightarrow$ X -gap	8.65	–45.96	2.65
$\Gamma \rightarrow$ L -gap	–8.50	45.155	–2.604
$\Gamma \rightarrow \Gamma$ -gap	3.02	–16.04	9.25
Previous study $\Gamma \rightarrow$ X [13]		–24.06	
BeSe			
$\Gamma \rightarrow$ X -gap	11.979	–37.42	2.80
$\Gamma \rightarrow$ L -gap	–15.80	49.358	–3.701
$\Gamma \rightarrow \Gamma$ -gap	3.193	–9.97	7.48
Previous study$\Gamma \rightarrow$ X [13]		–20.43	
BeS			
$\Gamma \rightarrow$ X -gap	13.24	–28.10	3.15
$\Gamma \rightarrow$ L -gap	–17.50	37.143	–3.425
$\Gamma \rightarrow \Gamma$ -gap	3.41	–7.24	6.68
Previous study $\Gamma \rightarrow$ X [12]		–21.7	
Previous study $\Gamma \rightarrow$ X [13]		–16.62	
Previous study $\Gamma \rightarrow$ L [12]			
Previous study $\Gamma \rightarrow \Gamma$ [12]		–8.87	

modulus B_0 in equation (1), the band gap pressure coefficients are determined. These are also tabulated in Table 3. It is found that in Figure 4, the indirect (Γ–X) and direct ($\Gamma - \Gamma$) band gaps (E_g) generally decrease with increase in pressure, thus BeX (X = Te, Se, S) have negative pressure coefficient ($\frac{dE_g^\alpha}{dP}$) ($\alpha = \Gamma$–X and $\Gamma - \Gamma$) (see Tab. 3, col. 3). On the other hand, the indirect ($\Gamma - L$) band gap (Fig. 4b) increases with increase in pressure giving rise to positive band gap pressure coefficient. For both the indirect and direct band gaps, the magnitude of the pressure coefficient decreases with increase in anion atomic number. Our results are in good agreement with the available theoretical results [12,13].

It is interesting to note the difference between the variation of the indirect and direct band gaps for volumes greater than the calculated equilibrium volumes. The band gaps deviate from being linear as displayed in Figure 4 above the equilibrium volume. The indirect band gaps (Figs. 4a and 4b) show smaller deviation compared to those of direct band gaps displayed in Figure 4c. The direct band gaps decrease abruptly for volumes larger than the equilibrium volume of the compound.

We can also account for the effect of changes in volume on the band gap by calculating the volume deformation potential (a_v^α) using [33]

$$a_v^\alpha = \frac{dE_g^\alpha}{d\ln V} = -B_0 \frac{dE_g^\alpha}{dP}, \qquad (12)$$

where B_0 is the bulk modulus. The results are given in Table 3. We note that for the beryllium compounds, $\frac{dE_g^\alpha}{d\ln V}$ increases as the anion atomic number decreases for $\alpha = \Gamma$–X indirect band gap while for the direct $\alpha = \Gamma - \Gamma$ band gap, the deformation potential decreases with decrease in anion atomic number. This means that as the ionicity of the compound increases from BeTe to BeS, the volume deformation potential for the indirect (Γ–X) and direct ($\Gamma - \Gamma$) band gaps increases and decreases respectively.

Another way of representing the effect of pressure on the band gap is through the use of a second-order polynomial fit [34–36] to the calculated values with

$$E_g^\alpha(a) = E_g^\alpha(a_0) + B\left(\frac{-\Delta a}{a_0}\right) + C\left(\frac{-\Delta a}{a_0}\right)^2 \qquad (13)$$

where Δa is the change in the lattice constant, a_0 the equilibrium lattice spacing and α is either the indirect $\Gamma - X$, $\Gamma - L$ or direct $\Gamma - \Gamma$ band gap. The values of the coefficients obtained from this quadratic fit are tabulated in Table 4. Figures 5a–5c show the calculated variation of the band gaps with the relative variation in lattice constant. It is seen that theoretically, the indirect band gap ($\Gamma - X$) decreases with increase in the relative change of the lattice constant for all the compounds since both coefficients B and C are negative (see Tab. 4). This is in agreement with the variation of the band gap with lattice constant deduced for GaAs [36]. Contrary to this behaviour, is that exhibited by the gap due to the $\Gamma - L$ transition. This gap increases with the increase in the relative variation of in the lattice constant (Fig. 5b) for all the beryllium monochalcogenides. An interesting response to the application of pressure is exhibited by the direct $\Gamma - \Gamma$ band gap.

Table 4. Coefficients obtained from least-square fits with $E_0(a) = E_0(a_0) + B(-\frac{\Delta a}{a_0}) + C(-\frac{\Delta a}{a_0})^2$ to the calculated values of the indirect $\Gamma \rightarrow$ X, $\Gamma \rightarrow$ L and direct $\Gamma \rightarrow \Gamma$ band gaps of beryllium chacogenides, BeTe, BeSe and BeS.

	$E_0(a_{expt})$ (eV)	B (eV)	C (eV)
BeTe			
$\Gamma \rightarrow$ X -gap	2.027	–7.087	–21.897
$\Gamma \rightarrow$ L -gap	3.048	8.199	7.311
$\Gamma \rightarrow \Gamma$ -gap	3.636	8.889	–249.523
BeSe			
$\Gamma \rightarrow$ X -gap	2.675	–6.173	–22.009
$\Gamma \rightarrow$ L -gap	4.258	10.554	11.860
$\Gamma \rightarrow \Gamma$ -gap	4.224	18.496	–85.780
BeS			
$\Gamma \rightarrow$ X -gap	3.149	-6.420	–26.581
$\Gamma \rightarrow$ L -gap	5.401	10.369	–8.311
$\Gamma \rightarrow \Gamma$ -gap	5.656	10.377	–366.516

This gap initially increases with the relative variation in the lattice constant, before it shows a down turn after reaching a peak value. This is more prominent in BeS and BeTe. This trend, (also seen with similar calculations using local density approximation), is contrary to the linear variation reported in reference [15], although they used a different experimental lattice constant.

From our band structure studies, the behaviour of the indirect ($\Gamma - X$, $\Gamma - L$) and direct ($\Gamma - \Gamma$) band gaps can be understood in terms of the relative changes in the energies of the various bands as pressure is varied. It is found that in these compounds, the indirect band($\Gamma - X$) gap decreases with increase in pressure due to the lowering in energy of the conduction band (Be p and chalcogen d_{eg}) at that point. On the other hand, the $\Gamma - L$ gap increases as the pressure is increased because energy of the conduction band (anion s) at the L point increases. The two indirect band gaps therefore respond differently to application of pressure. For the direct ($\Gamma - \Gamma$) band gap pressure dependence, there is a kink in the data associated with the application of pressure in all the three materials. This probably arises from band mixing among lower conduction bands at the Γ-point when the lattice constant is changed. It is seen that the decrease in the band gap with increase in pressure arises as a result of the closing of the gap between the lowest conduction band and the next higher doubly degenerate band at the Γ point leading to triple degeneracy. On further increasing the pressure, the triple degeneracy at the Γ point on the conduction band breaks, giving rise to a doubly degenerate(lower) and a single next higher band at this point. As this gap increases, a reduction in the direct $\Gamma - \Gamma$ band gap with increase pressure is observed.

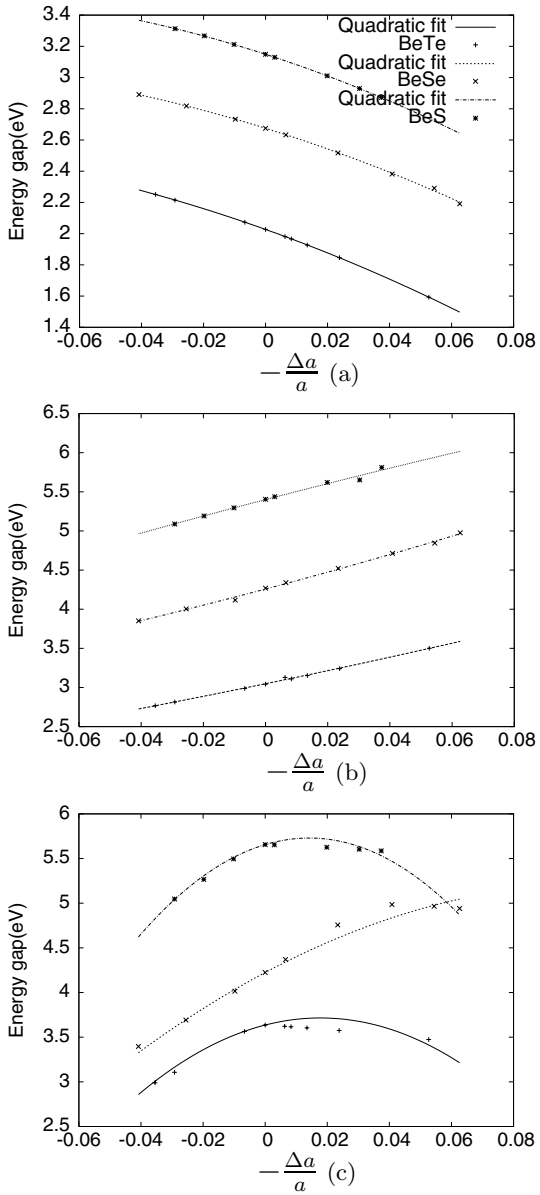

Fig. 5. Theoretical dependence of the (a) indirect ($\Gamma_v - X_c$) band gap, (b) ($\Gamma_v - L_c$) and (c) direct ($\Gamma_c - \Gamma_c$) for beryllium chalcogenides: (a) BeTe (b) BeSe and (c) BeS as a function of relative variation of lattice constant. The lines represent the the quadratic fit to the theoretical values using parameters in Table 4. The legend for (a) also applies to (b) and (c).

4.1 Optical properties

We have used equations (4–11) to calculate the optical properties scalar relativistically in this study. The calculated spectra have been rigidly shifted in order to correct for the DFT underestimation of the band gaps. We perform the scissors operator by an upward shift in energy of ε_2 by 0.366 eV, 0.218 eV for BeTe and BeSe. The estimates of the shift were obtained by ensuring that the maxima of the calculated imaginary part of the dielectric function coincide with the maxima of the measured spectra [38]. For BeS, no scissors shift was performed due to

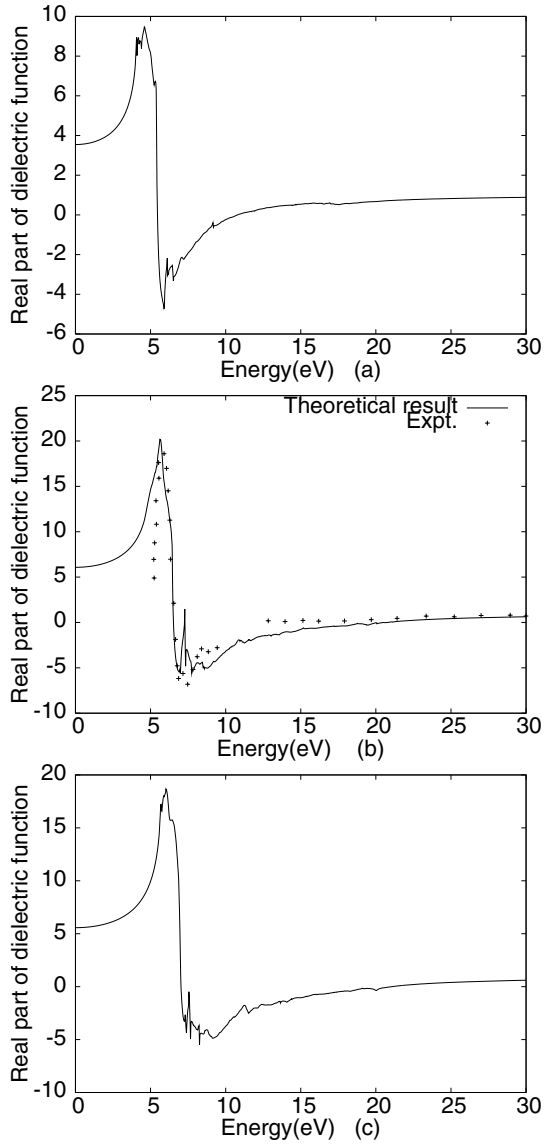

Fig. 6. Calculated real parts of dielectric function for (a) BeTe, (b) BeSe and (c) BeS.

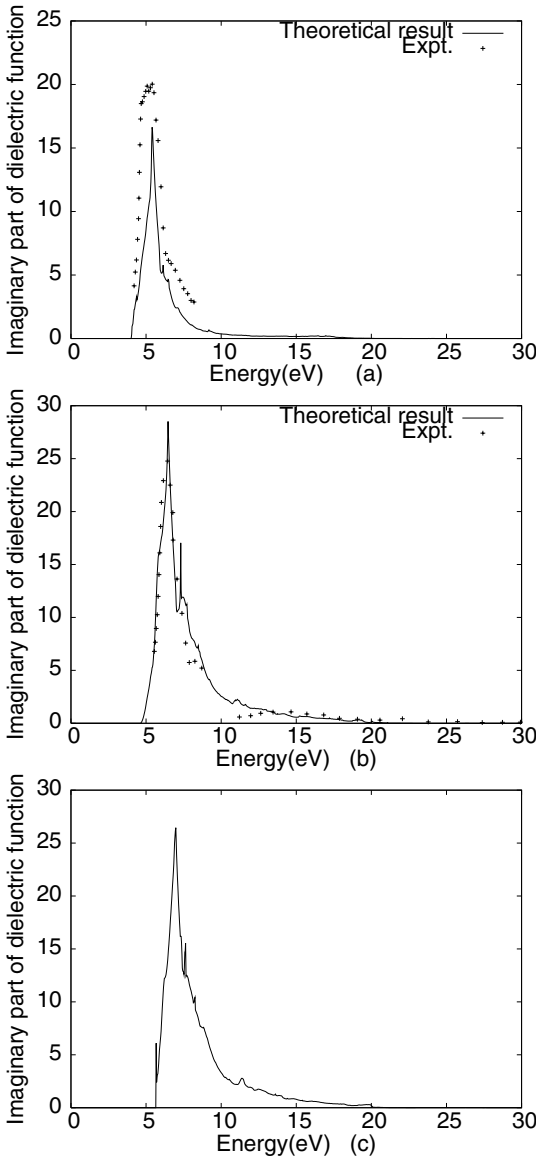

Fig. 7. Calculated imaginary parts of dielectric function for (a) BeTe, (b) BeSe and (c) BeS.

non availability of experimental measurements. The optical spectra calculated for the three compounds are displayed in Figures 6–12. In Figures 6 and 7 are the real, (ε_1) and imaginary, (ε_2) parts of the dielectric function in the energy range 0 and 30.0 eV. Generally, It is seen that the dielectric spectra for the beryllium chalcogenides appear similar. The real part of the dielectric function $\varepsilon_1(\omega)$ are shown in Figure 6. It is interesting to note that the first peak in $\varepsilon_1(\omega)$ coincides with the transition at the point L between the top of the valence band and the bottom of the conduction band. The major difference between the $\varepsilon_1(\omega)$ spectra of the compounds appear to occur in the region where $\varepsilon_1(\omega)$ is negative with BeS exhibiting the least of sharp structures in the region. It is found that the peak intensity in the dielectric function is highest in BeSe. and occur at 4.62 eV, 6.57 eV and 6.03 eV for BeTe, BeSe and BeS respectively. These correspond to direct interband transitions which originate from the top of the valence band at the L-point to the lowest conduction band. The imaginary part of the dielectric function for the compounds are also shown in Figure 7. The onset of the absorption edge in ε_2 occurs at 4.01 eV, 4.60 eV and 5.65 eV in BeTe, BeSe and BeS. These correspond to the direct optical band gap($\Gamma_v \rightarrow \Gamma_c$). In all the compounds, their is a sharp increase in the slope of ε_2 beginning at the optical band gap and rising to the main peak. The global peak in ε_2 occurs at 5.44 eV, 6.50 eV and 6.98 eV for BeTe, BeSe and BeS respectively. This is followed by small structures at 7.31 eV and 7.64 eV in BeSe and BeS respectively. These small structures arise due to direct transitions from the top of the valence band at the L-point to the next higher conduction band ($L_{3v} \rightarrow L_{3c}$) in the compounds. Our calculated ε_2 spectra compare very well with those of Stukel [9].

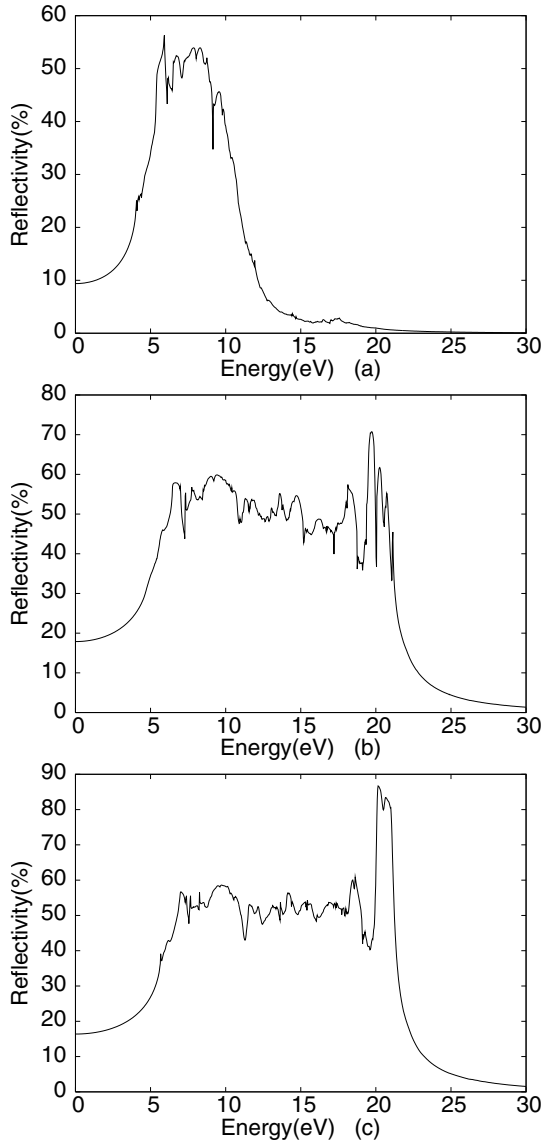

Fig. 8. Calculated reflectivity of (a) BeTe, (b) BeSe and (c) BeS.

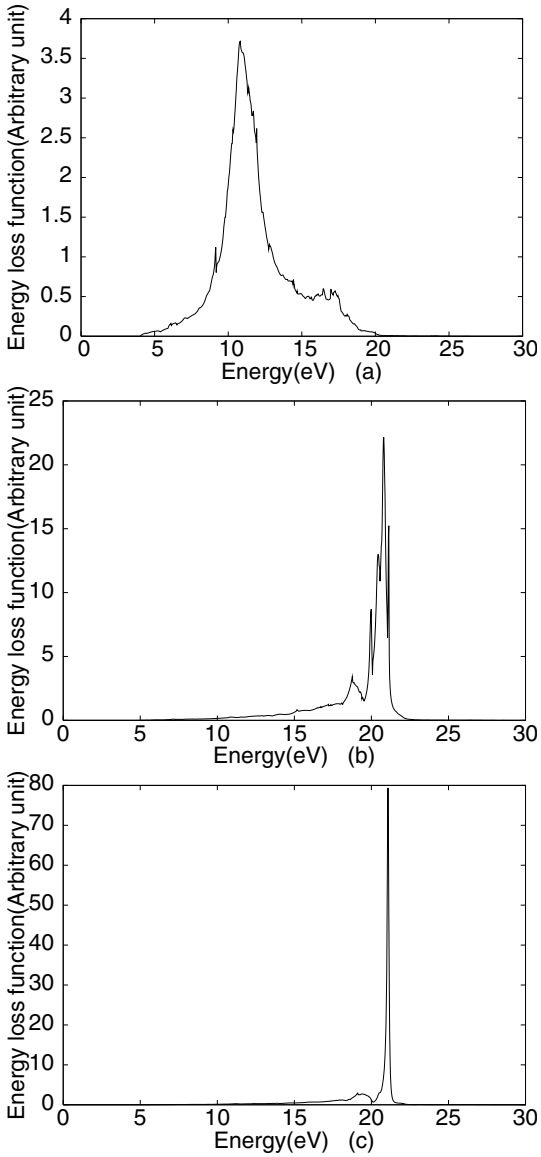

Fig. 9. Calculated electron energy-loss function of (a) BeTe, (b) BeSe and (c) BeS.

In Figure 8, we exhibit the calculated reflectivity spectra for the compounds using equation (6). We note that in the three compounds, the reflectivity spectra is small in the low energy region indicating that interband transitions do not occur in the far infrared (IR) spectrum in these large band gap semiconductors. Hence, they reflect more from the ultra violet region especially in BeSe and BeS. On the whole, the reflectivity spectra obtained for the three compounds show that the reflectivity is on the average generally between 9% and 60% up to 12 eV for BeTe and 22 eV for both BeSe and BeS, except for some few small peaks. Beyond these energies, the reflectivity drops sharply. The behavior of the reflectivities between ∼7–23 eV for BeSe and BeS and between 5–12 eV for BeTe, make the compounds particularly good for applications in visible and ultra violet region.

The electron energy loss-function for beryllium chalcogenides BeTe, BeSe and BeS are displayed in Figure 9. The spectra displayed in Figure 9 show that the loss function for BeTe is different from those of BeSe and BeS because of the wider width of the peak. This function is usually large at the plasmon energy whose position corresponds to $\varepsilon_1(\omega) = 0$, provided $\varepsilon_2(\omega)$ is reasonably smooth in these regions [39,40]. In these compounds, at around 10.8 eV, 20.8 eV and 21.1 eV for BeTe, BeSe and BeS respectively, the energy loss spectra exhibit a large peak.

The calculated linear absorption spectra are plotted in Figure 10 for BeTe, BeSe and BeS. The general profile of their frequency dependence are similar especially for BeSe and BeS. For all the compounds the onset of absorption involves a sharp increase in the spectra at energies corresponding to the fundamental optical gap. This indicates that BeTe, BeSe and BeS have the same mechanism of

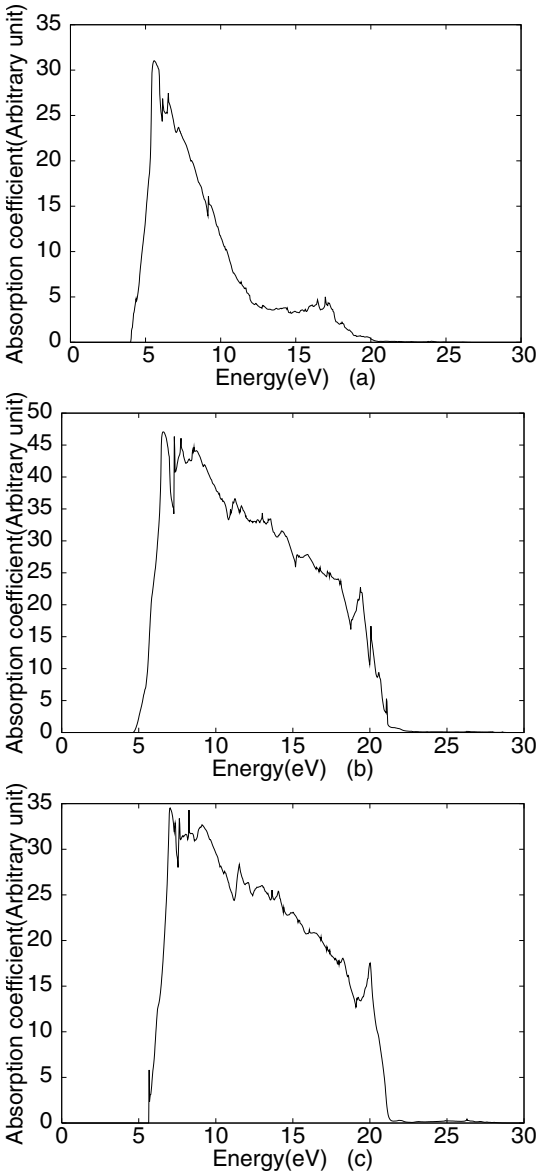

Fig. 10. Calculated linear absorption coefficient of (a) BeTe, (b) BeSe and (c) BeS.

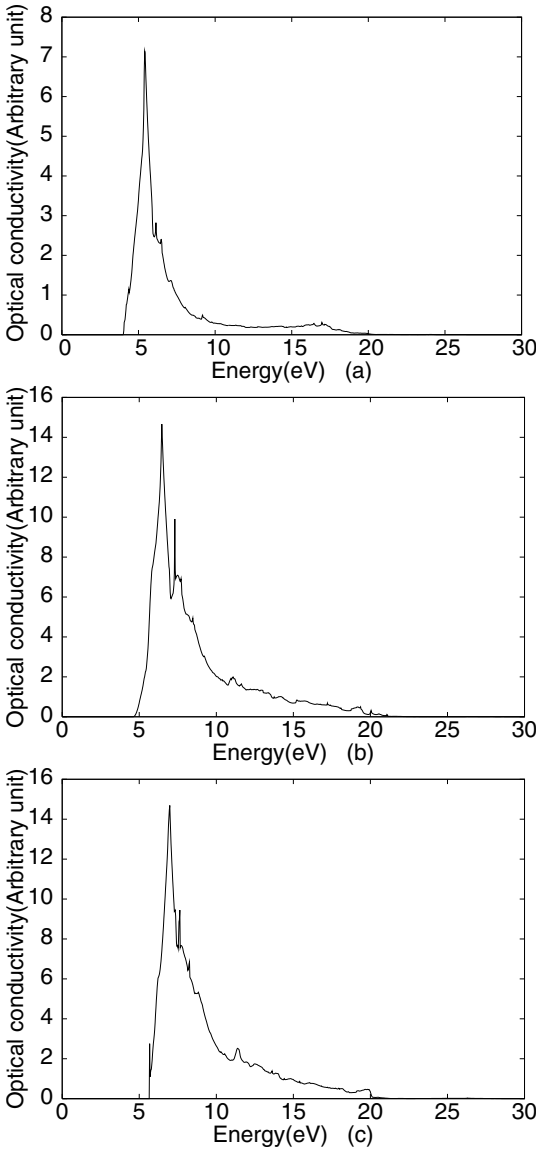

Fig. 11. The theoretical real part of optical conductivity of (a) BeTe, (b) BeSe and (c) BeS.

optical transition at these energy positions. In the BeTe absorption spectra, after attaining the peak, there is a relatively sharper decrease than in BeSe and BeS. The spectra also exhibit a unique shoulder between 14.8 and 17.5 eV. This might be due to the presence of anion d electrons in the conduction band structure. This feature does not appear in the other compounds (BeSe and BeS).

In Figure 11, the calculated real part of the optical conductivity in beryllium chalcogenides BeTe, BeSe and BeS are displayed. After a start of a smooth and zero conductivity, we obtain a sharp increase that reaches a peak at 5.4 eV, 5.42 eV and 6.98 eV for BeTe, BeSe and BeS respectively, before dropping rapidly. It is known that the real part of optical conductivity of a system is directly proportional to the product of energy and the imaginary part of the dielectric function ε_2. As such, the origin of the structures in the imaginary part of the dielectric function also explain those of the optical conductivity. The relative amplitudes of the structures scale as $\omega\varepsilon_2$.

In Figures 12a–12c, the calculated refractive index (solid line) and the extinction coefficient (dotted lines) are plotted. The general profiles of the refractive index and extinction coefficient spectra of the compounds are quite similar. However, the energy at which the refractive index and extinction coefficient cross in all the compounds increases from BeTe to BeS. The refractive index and extinction coefficient spectra of the compounds have resonance in the ultra violet which corresponds to the interband transitions. We also note that the refractive index of all the compounds lie between 1.9 and 2.5 in the far infrared region, while in the hard ultra violet region, the refractive index has normal dispersion since it increases with energy in the transparency region (1.5–3 eV).

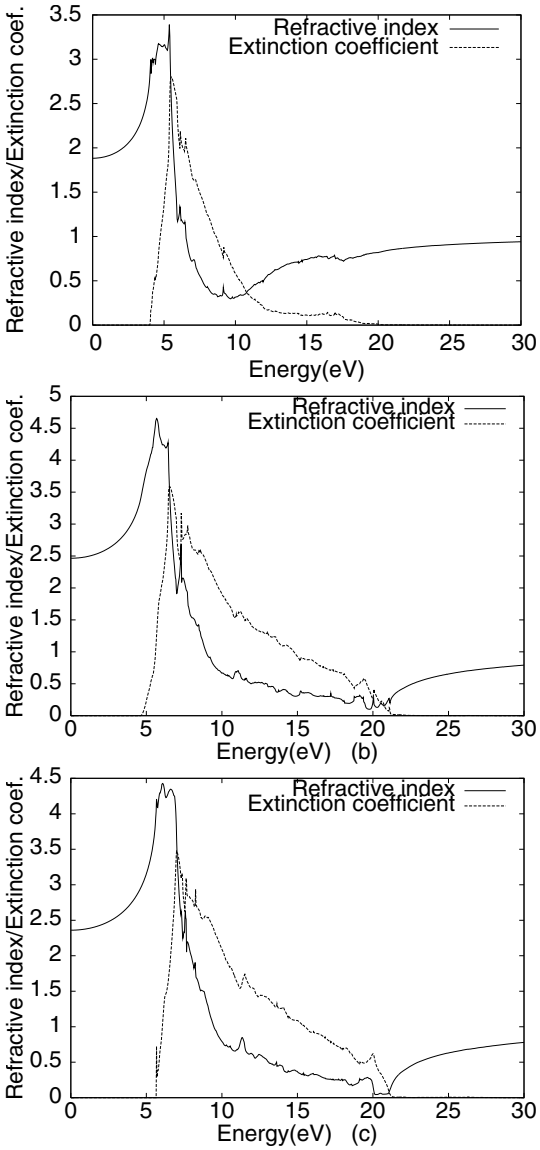

Fig. 12. The refractive index (continuos line), extinction coefficient (dotted line) of (a) BeTe, (b) BeSe and (c) BeS.

5 Conclusions

We have used the generalized gradient approximations within the full potential linearized augmented plane wave method to study the structural, electronic and optical properties of zincblende beryllium monochalcogenides, BeTe, BeSe and BeS. Our results show that generally the effect of the increase in the anion charge of these compounds to the band structure, is to decrease the band gaps as well as the valence band width. Our investigation of the effect of pressure on the direct and indirect band gaps of the compounds show that they respond differently to the application of pressure. The direct and indirect band gap pressure coefficient for the compounds are all negative and in both cases decrease with increase in anion atomic number. Also, we found that for the direct $(\Gamma - \Gamma)$ band gap, the deformation potential decreases as the chalcogen atomic number decreases while it increases with decrease in anion atomic number for the indirect band gap. The results of our calculations of the dielectric functions compares very well with available experimental measurements. The reflectivity is found to have a maximum of about 60% in all the compounds. The agreement between our calculations and the ellipsometry measurements for the dielectric function gives credence to the results on the other calculated optical properties for which no experimental data are available.

The author would like to thank P. Blaha, K. Schwarz and J. Luitz for providing the WIEN97 code. My thanks also go to the International Atomic Energy Agency and UNESCO for hospitality at the Abdus Salam International Center for Theoretical Physics (ICTP), Trieste, Italy. Financial support of the Swedish International Development Cooperation Agency (SIDA) during my visit to ICTP as a regular associate is acknowledged.

References

1. H. Luo, K.Ghandehari, R.G Greene, A.L. Ruoff, S.S. Trailand, F.J. DiSalvo, Phys. Rev. B **52**, 7058 (1995)
2. J.A. Vechten, Phys. Rev. **187**, 1007 (1969)
3. A. Waag, F. Fischer, H.J. Lugauer, Th. Litz, J. Laubender, U. Lunz, U. Zhender, W. Ossau, T. Gerhardt, M. Moller, G. Landwehr, J. Appl. Phys. **80**, 792 (1996)
4. W.M. Yim, J.B. Dismakes, E.J. Stofko, R.J. Paff, J. Phys. Chem. Solids **33**, 501 (1972)
5. E. Staritzky, Anal. Chem. **28**, 915 (1956)
6. W. Zachariasen, Z. Physik Chem. (Leipzig) **119**, 210 (1926); **124**, 440 (1926)
7. K. Wilmers, T. Wethkamp, N. Esser, C. Cobet, W. Richter, V. Wagner, A. Waag, H. Lugauer, F. Fisher, T. Gerhard, M. Keim, M. Cardona, Phys. Stat. Solidi (b), **215** 15 (1999)
8. K. Wilmers, T. Wethkamp, N. Essar, C. Cobet, F. Richter, V. Wagner, H. Lugauer, F. Fischer, T. Gerhard, M. Keim, Phys. Rev. B **59**, 10071 (1999)
9. D.J. Stukel, Phys. Rev. B **2**, 1852 (1970)
10. R.L. Sarkar, S. Chatterjee, J. Phys. C **10**, 57 (1977)
11. A. Munoz, P. Rodriguez-Hernandez, A. Mujica, Phys. Stat. Solidi (b) **198**, 439 (1996); A. Munoz, P. Rodriguez-Hernandez, A. Mujica, Phys. Rev. B **54**, 11861 (1996)
12. P.E. Van Camp, V.E. Van Doren, Solid State Commun. **98**, 741 (1996)
13. M. Gonzalez-Diaz, R. Rodriguez-Hernandez, A. Munoz, Phys. Rev. B **55**, 14043 (1997)
14. A. Fleszar, W.Hanke, Phys. Rev. B **62**, 2466 (2000)
15. N. Benosman, A. Amrane, S. Mecabih, H. Aourag, Physica B **304**, 214 (2001)
16. A. Deb, M. Itoh, Y.Sakurai, N. Hiraoka, N. Sakai, Phys. Rev. B **63**, 064409 (2001)
17. P. Blaha, K. Schwarz, J. Luitz, WIEN97, Vienna University of Technology, 1997 [Improved and updated Unix version of the original copyrighted WIEN-code], which was published by P. Blaha, K. Schwarz, P. Sorantin, S.B. Trickey in: Comput. Phys. Commun. **59**, 399 (1999)

18. J.P. Perdew, S. Burke, M. Ernzerhof, Phys. Rev. Lett. **77**, 3865 (1996); J.P. Perdew, S. Burke, M. Ernzerhof, Phys. Rev. Lett. **78**, 1396(E) (1997)
19. P. Hohenberg, W. Kohn, Phys. Rev. **136**, 864 (1964); W. Kohn, L.J. Sham, Phys. Rev. A **140**, 1133 (1965)
20. M. Lach-hab, M. Keegan, D.A. Papaconstantopoulos, M.J. Mehl, J. Phys. Chem. Solids **61** (2000) 1639; M. Lach-hab, M. Keegan, D.A. Papaconstantopoulos, M.J. Mehl, J. Phys. Chem. Solids **61** 1639 (2000)
21. C. Ambrosch-Draxl, R. Abt, *The Calculation of optical properties within WIEN97* (1998) ICTP Lecture Notes (unpublished)
22. Y.P. Yu, M. Cardona, *Fundamentals of semiconductors: Physics and materials properties*, 2nd edn. (Springer-Verlag, Berlin, 1999)
23. A. Delin, A.O. Eriksson, R. Ahuja, B. Johansson, M.S.S. Brooks, T. Gasche, S. Auluck, J.M. Wills, Phys. Rev. B **54**, 1673 (1996); P. Ravindran, A. Delin, B. Johansson, O. Eriksson, J.M. Wills, Phys. Rev. B **59**, 1776 (1999); P. Ravindran, A. Delin, P. James, B. Johansson, J.M. Wills, R. Ahuja, O. Eriksson, Phys. Rev. B **59**, 15680 (1999)
24. M. Fox, *Optical Properties of Solids* (Oxford University Press, New York, 2001)
25. M. Dressel, G. Gruner, *Electrodynamics of solids: optical properties of electrons in matter* (Cambridge University Press, UK, 2002)
26. F.D. Murnaghan, Proc. Natl. Acad. Sci. USA **30**, 244 (1944)
27. S.-H. Wei, A. Zunger, Phys. Rev. B **53**, R10457 (1996)
28. S.-H. Wei, A. Zunger, J. Appl. Phys. **78**, (1995) 3846 and refrerences therein
29. M.S. Hybersten, S.G. Louie, Phys. Rev. Lett. **55**, 1418 (1985); M.S. Hybersten, S.G. Louie, Phys. Rev. B **34**, 5390 (1986); X. Zhu, S.G. Louie, Phys. Rev. B **43**, 14142 (1991); R.W. Godby, M. Schluter, L.J. Sham, Phys. Rev. Lett. **56** 2415 (1986); R.W. Godby, M. Schluter, L.J. Sham, Phys. Rev. **35**, 4170 (1987); R.W. Godby, M. Schluter, L.J. Sham, Phys. Rev. **37**, 10159 (1988)
30. S. Fahy, K.J. Chang, S.G. Louie, M.L. Cohen, Phys. Rev. B **35**, 5856 (1987)
31. M.S. Hybertsen, S.G. Louie, Phys. Rev. Lett. **55**, 1418 (1985)
32. B. Bouhafs, H. Aourag, M. Certier, J. Phys.: Condens. Matter **12** 5655 (2000)
33. Z. Dridi, B. Bouhafs, P. Ruterana, New J. Phys. **4**, 94.1 (2002)
34. Su -Huai, A. Zunger, Phys. Rev. B. **60**, 5404 (1999)
35. A. Continenza, S Massida, A.J. Freeman, Phys. Rev. B **38**, 12996 (1988)
36. E. Ghahramani, J.E. Sipe, Phys. Rev. B **40**, 12516 (1989)
37. C.O. Rodriguez, E.L. Peltzer y Blanca, O.M. Cappannini, Phys. Rev. B **33**, 8436 (1985)
38. A. Delin, P. Ravindran, O. Eriksson, J.M. Wills, Int. J. Quant. Chem. **69**, 349(1998)
39. C.S. Wang, B.M. Klein, Phys. Rev. B **24**, 3417 (1981)
40. J.H. Simmons, K.S. Potter, *Optical materials* (Academic Press, San Diego, 2000)